12-2007

A CFD Investigation of Axisymmetric Microthruster Nozzles for use on Nano-Satellites

Michael R. O'Gara
Embry-Riddle Aeronautical University - Daytona Beach

A CFD INVESTIGATION OF AXISYMMETRIC MICROTHRUSTER NOZZLES FOR USE ON NANO-SATELLITES

Michael R. O'Gara

Master of Science Aerospace Engineering

Embry-Riddle Aeronautical University

Daytona Beach, Florida

December 2007

A CFD INVESTIGATION OF AXISYMMETRIC MICROTHRUSTER NOZZLES FOR USE ON NANO-SATELLITES

by

Michael R. O'Gara

This thesis was prepared under the direction of and approved by the members of the candidate's thesis committee. It was submitted to the Aerospace Engineering Department and was accepted in partial fulfillment of the requirements for the degree of Master of Science in Aerospace Engineering.

THESIS COMMITTEE:

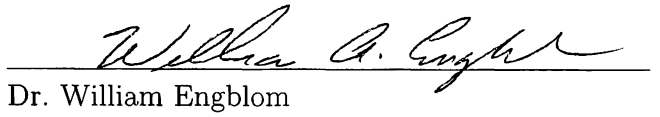

Dr. William Engblom
Co-Chairman

Dr. Vladimir Golubev
Co-Chairman

Dr. Reda Mankbadi
Member

Dr. Habib Eslami
Department Chair, Aerospace Engineering

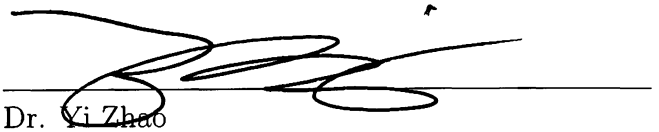

Dr. Yi Zhao
Program Coordinator, Aerospace Master's Program

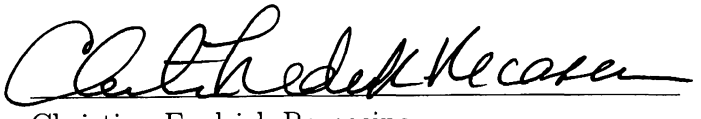

Christina Fredrick-Recascino
VP for Research and Institutional Effectiveness

10-17-07
Date

ACKNOWLEDGEMENTS

The author acknowledges the time and effort of his thesis committee members The author would like to especially thank Dr William Engblom for the inspiration and the direction given towards the completion of this thesis Recognition is also given to Dr Vladimir Golubev and Dr Reda Mankbadi for their interest shown on the subject

Appreciation is also given to Dr David Sypeck for his efforts in the experimental process as well as to Dr Nicholas Georgiadis of NASA Glenn Research Center and Dr Christopher Nelson of Innovative Technology Applications Center for their technical expertise regarding the WIND-US flow solver

Lastly, the author thanks his family and friends for their unwavering support and encouragement through the duration of the masters degree completion

ABSTRACT

The performance of microthruster nozzles ($\sim$ 0.1 N thrust) depending on nozzle contour, propellant and surroundings, destined for use in nanosatellite missions, is investigated via a numerical approach using the Wind-US flow solver. An experimental apparatus designed to measure microthruster performance in atmospheric or vacuum conditions used to aid numerical simulations is also presented. Comparing the numerical and experimental results show an approximate 25% drop in efficiency for unknown reasons. An evaluation of favorable nozzle contours suggested by previous researchers is conducted, and the results demonstrate the need for a more rigorous treatment of the nozzle flow at the exit plane. A matrix of numerical simulations of conical and bell nozzles using Wind-US are presented which indicate optimum thrust performance as function of conical half angle, bell nozzle exit angle, and geometric scale. Correlations are provided for optimum micronozzle thrust efficiency versus throat Reynolds number, along with optimal shape.

TABLE OF CONTENTS

LIST OF TABLES

LIST OF FIGURES

INTRODUCTION

Subject Interest

Microthruster monopropellant and cold gas systems are an attractive option for nano-satellite applications. Monopropellant systems typically offer larger specific impulse than cold gas systems as well as reduced tank mass and leak rates due to lower supply pressures. Monopropellant systems also require significantly less power than electric thruster systems, a resource highly limited on nano-satellites. MEMS-based systems are still in development and have limitations in terms of complete catalytic decomposition of propellant and rectangular nozzle fabrication issues. The issue of nozzle performance due to intensified viscous effects at the micro scale is fundamental to the design of future microthruster systems.

It is useful to consider recent examples of nano-satellite propulsion impulse requirements. Mueller[10] defined minimum impulse bits (I-bit) required for typical microspacecraft missions. For a 10 kg spacecraft, an I-bit would be 0.14 mN-s for a firing duty cycle of 20 Hz and 1 degree pointing. These requirements are needed for maneuvering and orientation of the spacecraft to complete its assigned mission. University teams around the world are building nano-satellites that meet the Cubesat specifications defined by Cal Poly University.[3] These specifications are for a satellite 10 cm on a side (the shape of a cube) and a total system mass of 1 kilogram. Storck and colleagues[15] described very basic needs for a micropropulsion module for these spacecraft. Their requirements were for a system with an impulse bit of 1.0 mN-s. The MagCon nanospacecraft constellation, studied by NASA

Goddard Space Flight Center, is designed to use nanospacecraft with mass of no more than 10 kg to observe the Earths magnetosphere environment.[13] The attitude control parameters for this mission are 2.4 N-s total mission impulse, an input power less than 1 watt, specific impulse of 60 seconds, and minimum impulse bit of no more than 44 mN-s. Thrust levels of milli-newtons to tenths of newtons are commonly cited for micropropulsion systems such as those listed above.

Previous Studies

An important consideration towards achieving high microthruster performance is the nozzle scale and contour. The enhanced role of viscous effects renders traditional methods of optimization invalid as these are based on the method-of-characteristics (e.g., Rao[12]). A standard approach for large-scale nozzle design is to correct a truncated ideal nozzle contour (i.e. the MOC result) for viscous effects by accounting for the altered effective shape of the inviscid core flow due to turbulent boundary layer growth. However, this approach is generally not applicable to micronozzles, since the boundary layer thickness tends to be a large fraction of the entire nozzle flowfield. An evaluation based on the Navier-Stokes equations is required, provided the continuum flow assumption holds. As the nozzle scales down heat transfer effects and surface roughness effects also become considerations. Extremely small scales (e.g., throat on the order of tens of microns) will produce Reynolds numbers below 200 and free molecular flow becomes prevalent.[7] An early attempt to numerically optimize the performance of both conical and bell-shaped nozzle contours for a low Re^* micronozzle was conducted by Hussaini and Korte.[5] This methodology involved use of a combination of full Navier-Stokes and parabolized Navier-Stokes solvers to compute the flowfield inside a nozzle until the exit plane. The flow solver was linked to an optimizer for which the objective function was the thrust under vacuum conditions. The authors

concluded that a CFD-based optimization produces an improved design compared to the traditional MOC-based approach. The authors numerical technique identified a rather odd-looking contour shape for the optimal bell nozzle performance, including a 20° inward turning angle at the nozzle exit (as opposed to conventional 0° angle). Shebalin and Tiwari[14] conducted a more rigorous optimization of both conical and bell micronozzles using a CFD-based optimization system which included the NASA-developed Vulcan flow solver and commercial optimization software, ISIGHT. Similar results were obtained, including the same inward turning bell shaped nozzle reported in Ref. 5. Another interesting feature that results from this optimized nozzle is an area of recirculation near the exit of the nozzle where the overall nozzle radius extends beyond the exit radius (discussed later).

Unfortunately, no experimental evaluation of these results has been offered to date. This may be due in part to the realization that precise measurement of typical micronozzle thrusts (e.g., 0.1 N) during vacuum operation presents significant technical challenges. More recent evaluations have focused on MEMs-type linear micronozzles. For example, Louisos and Hitt[9] focus on the performance of 2-D MEMs-type linear micronozzles. They demonstrate the strong sensitivity of micronozzles to viscous effects and find an optimal expansion angle of 25-30 degrees. These two have also discussed the effect of heat transfer on the viscousity of the flow, concluding that the heat loss from the flow results in better performance.[8] A 3-D investigation of MEMs-type nozzles is conducted by Jones and Mattick[6] which addresses the effect of combustion on nozzle performance. Bayt[2] provides an array of numerical and experimental thrust predictions for MEMstype nozzles, showing pronounced viscous effects at low Reynolds number. However, significant uncertainties are found regarding the provided experimental thrust stand measurement. It has also been reported that 2-D analysis of rectangular MEMS

nozzle geometries will produce significant errors compared to 3-D analysis due to the 3-D nature of rectangular nozzle flows and end wall effects.[1] It is apparent that 2-D analysis is only accurate for axisymmetric micronozzles, and that such nozzles will be more efficient than the linear-type nozzles for similar throat diameter, expansion ratio, etc., and thus represents an upper bound to performance. In many of the aforementioned references involving 2-D analysis, the numerical treatment of the nozzle outflow boundary as pure extrapolation, which as will be discussed shortly, introduces substantial uncertainty in evaluations at low Reynolds number. Consequently, the focus of this study is to provide an accurate model and correlation for predicting axisymmetric micronozzle performance.

Proposal

The numerical analysis will first support the work involved in the experimental testing of micronozzles. The numerical study will attempt to reproduce a similar optimal shape through the variation of half angle on a series of conical nozzles. The quantitative results from both the experimental and numerical analysis will be compared.

The second part of the proposed work for this thesis involves the investigation of the results obtained by Shebalin and Tiwari in Ref. 14. The first examination involving this work is the use of a single zone in their optimization study. Using the Wind-US code, the first task is to replicate the results which were presented. This involves the analysis of the inward turning nozzle using a single zone representing the interior of the nozzle. This study will be expanded by creating extra zones representing the plume area and marking the effects of these extra zones on the nozzle performance.

Once the proper treatment of the nozzle flow has been found, a new study to find the optimal shape of a micronozzle will be conducted. This study will not utilize an optimization code like the work in Ref. 14, but instead rely on a series of simulations of nozzles representing the optimal search domain. The results will be compared with the results found by Shebalin and Tiwari. After this initial investigation, the study will be expanded by changing the overall scale of the micronozzles and the propellent species to see the effect Reynold's number has on the nozzle performance. A correlation of the nozzle efficiency to Reynold's number and nozzle shape to Reynold's number is the final goal of this study.

EXPERIMENTAL SETUP

To measure small amounts of thrust in a vacuum and simulate the space environment, an experimental apparatus was obtained and assembled as shown in Fig. 1. The vacuum system consisted of a 150 mm ID glass tube chamber connected to a diffusion pumping station (Key High Vacuum Products, Nesconset, NY). With this system, levels of better than 10-6 Torr can be achieved. To measure thrust, a small 5 N capacity load cell (Instron Corporation, Norwood, MA) resides within the chamber. Fig. 2 provides an up close view of the load cell and micronozzle configuration. More details of the experimental apparatus and calibration can be found in Ref. 4.

Initial attempts to demonstrate the accuracy of the thrust stand for micronozzles involved conical nozzles with throat and exit diameters of 0.76 mm and 6.35 mm respectively, resulting in an area expansion ratio of 69. The half-angle was varied along with the length to maintain a constant expansion ratio. The nozzles were CNC machined from both PEEK (polyetheretherketones) and ultra machinable brass (alloy 360). However, microscopic inspection using a stereo zoom microscope revealed interior surface roughness and throat length/centricity that varied widely from nozzle to nozzle. Such variations would be difficult to accurately model using numerical methods. To allow direct comparison to numerical simulations, a single 30° half-cone angle nozzle was carefully drilled, inspected and deemed of sufficient quality. This new nozzle was made from ultra machinable brass with dimensions as those above. Note that the Re* of 76,628 implies potentially turbulent flow and high

thrust efficiency. This nozzle was tested in vacuum and sea-level back pressure conditions, using nitrogen gas at stagnation conditions of Po = 6 MPa and To = 300 K (unheated).

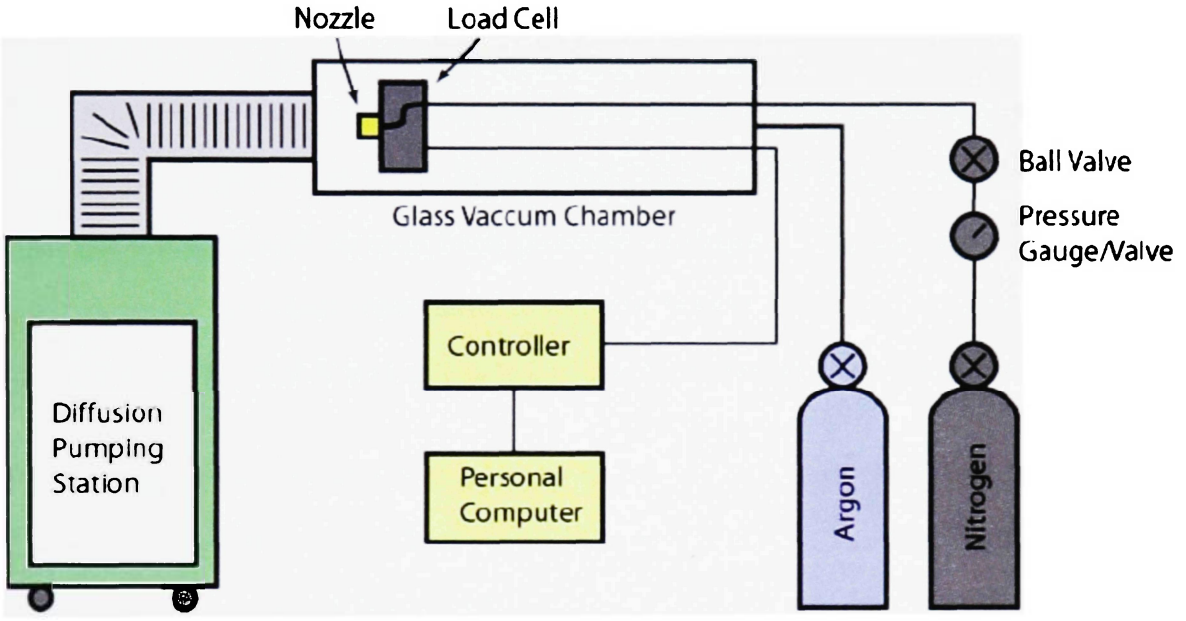

Figure 1: Setup for the experimental analysis

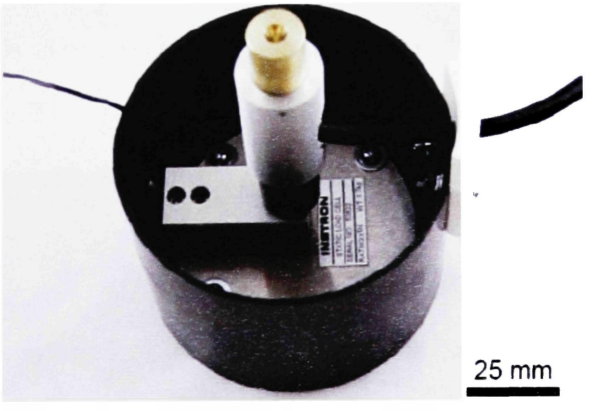

Figure 2: Close-up view of load cell and micronozzle

NUMERICAL SETUP

Methodology

The first task for the numerical analysis is to obtain results pertaining to the nozzle and conditions presented in the EXPERIMENTAL SETUP chapter. This includes both the sea level and vacuum back pressure conditions. The main focus of this study is to try to obtain reasonable agreement between the two methods for the 30° half-angle nozzle, which was machined to the best specifications possible.

The remainder of the numerical analysis will focus on the work of Shebalin and Tiwari provided in Ref. 14. As mentioned in the proposal, the first task regarding this paper is to replicate the thrust and flow pattern of the optimal bell nozzle featuring an inward turning nozzle. This will be accomplished through a boundary condition study of the outflow plane for a single, interior flow zone. Once similar results from Ref. 14 are obtained, the outflow condition will be removed by including an additional zone representing the plume region downstream of the nozzle exit plane. This senario should represent the flow characteristics with the most accurate results. The multi-zone results will be compared with the single-zone results to demonstrate which would be the preferred method for quick optimization of micronozzles.

The next focus of the numerical analysis will be to conduct a new optimization study. This will involve the creation of several micronozzles over the search domain and finding an approximate optimal shape based on the findings. This study will

adhere to the original study done by Shebalin and Tiwari in variation of the micronozzle shapes with the exception of the contoured nozzles. The study presented in Ref. 14 conducted a two variable optimization searching for the optimal exit angle and nozzle length. For the current study, the nozzle length is fixed to the optimal length (7.899 mm) found in Ref. 14, and the exit angle is the only parameter which was varied. For the conical nozzles, only the half angle and nozzle length are varied allowing the expansion ratio (and thus the exit diameter) to remain the same. Figures 3 and 4 show how the nozzles vary from one shape to another for the conical and bell nozzles respectively. Table 1 provides the constant geometric and aerodynamic values common to all the original simulations.

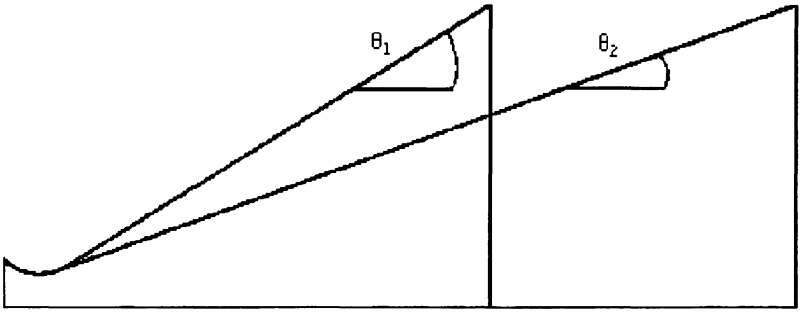

Figure 3: Variation of shape for conical nozzles

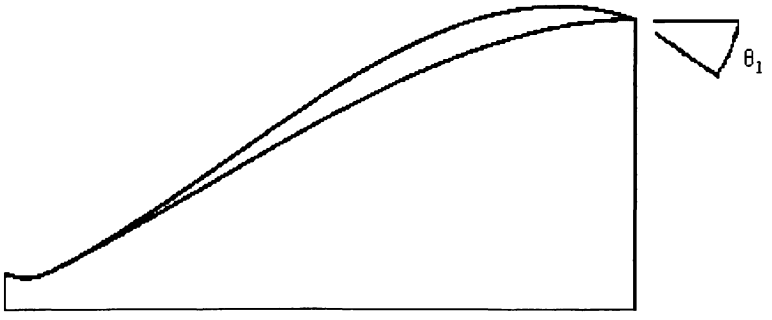

Figure 4: Variation of shape for bell nozzles

Table 1: Original Optimization Conditions

Parameter	
D*	0.84 mm
ϵ	82
P_0	150 kPa
T_0	1500 K

The effect Reynold's number has on the micronozzle's performance will be studied in two ways. The first will be to change the monopropellent species from the original hydgrogen gas (H_2) to nitrogen gas (N_2). This was accomplished by changing the coefficients found in Sutherland's Law which estimates viscosity. Equation (1) is Sutherland's Law and Table 2 provides the coefficients used for hydrogen and nitrogen. The second method of varying Reynold's number is through scale. Reducing the overall scale by $\frac{1}{2}$ effectively reduces the Reynold's number by this same amount. All of the angular dimensions however will remain the same, and the same analysis as the normal scale is performed again. Both of these methods will be used on the conical as well as the bell nozzles. Once an optimal shape is obtained for each of these changes, the results will be analyzed for a correlation between the Reynold's number and the nozzle's optimal efficiency and shape.

$$\mu = \frac{C_1 T^{(3/2)}}{(T + C_2)} \tag{1}$$

*where μ is in slug/ft-sec and T is in °R

Hardware and Software

The Wind-US flow solver is utilized for this effort. Wind-US is a general purpose flow solver provided by the NPARC Alliance, a partnership between NASA Glenn,

Table 2: Sutherland's law viscosity coefficients

Species	C_1	C_2
Hydrogen (H_2)	1.07361 $(10)^{-8}$	174.6
Nitrogen (N_2)	2.18009 $(10)^{-8}$	192.6

Air Force AEDC, and Boeing.[11] The Wind-US code has been extensively validated for a wide range of fluid physics. For the computations presented herein, inviscid fluxes are computed using a true 2nd order Roe scheme which accounts for grid stretching, and the solution is advanced using local time stepping (typically based on global CFL=0.5) and a spatially-split line-based factorization scheme. Laminar viscous effects are computed using central differencing and Sutherlands law for molecular viscosity. Convergence is based on monitoring mass and thrust histories and looking for $\sim 0.1\%$ variation over 1000 cycles or more.

The cluster's used for the simulations are housed in Embry-Riddle Aeronautical University's Lehman Building in Daytona Beach. Florida. The cluster Figaro has 11 nodes with 2 processors each for a total of 22 processors, each running at 1594 Mhz, for parallel computing. The Beowulf cluster has 262 64-bit processors running at 3.2 Ghz each. Both of these clusters were used to run multiple simulations simulataneosly with each simulation using a maximum of 2 processors. Results were typically obtained in less than a day from start to finish for each simulation.

Grid Generation

The grids of all the nozzles analyized using numerical methods take advantage of the axisymmetry of the geometry and flow characteristics. This allows the creation of a 2-D grid representing half of the lateral dimension of the nozzle and flowfield. Fig. 5

represents the grid of the nozzle interior for the inward turning bell nozzle. An input to Wind-US instructs the code to treat the flow as axisymmetic rather than 2-D.

The geometry of the experimental micronozzle was rather simple due to the presence of a sharp throat (no curvature). For this reason, the commerical software, GRIDGEN was used to generate the experimental nozzle grids. Due to the number of nozzles to be simulated and their geometric complexity at the throat, a different approach was considered for the nozzles provided in the Old Dominion study (Ref. 14).

To facilitate the grid generation process of the optimal shape study, a FORTRAN code was written and compiled. The code first creates the wall contour based upon the geometric characteristics of the nozzle given in Ref. 14. The conical and bell nozzles both have the same radius of curvature at the throat section and initial throat diameter. The inflection point where the radius of curvature starts and the bell nozzle contour begins remained fixed at 26° The inflection point on the conical nozzles marked the beginning of the straight wall section of the nozzle and was variable dependent upon the half angle. After the inflection point is located, the nozzle contour was calculated. This was achieved for the conical nozzles through basic trigonometry. The bell nozzle contour was created using a third order polynomial. Ref. 14 provides the nessessary equations to solve for the coefficients of the polynomial based upon the nozzle dimensions.

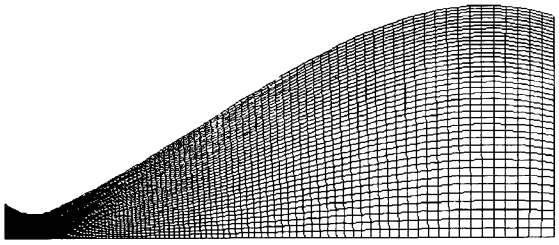

Figure 5: Sample grid of nozzle interior (every other grid point removed)

Once the wall contour is generated, the interior mesh is created. This is accomplished by setting of overall dimensions of the grid, as well as grid spacing at the throat and wall locations. Once these numbers are set, the code attempts to create the mesh through linear and geometric spacing schemes moving longitudinally from the throat to the entrence and exit planes and laterally from the wall down to the axisymmetric boundary. Through a study of different grid sizes, a suitable combination of throat and wall grid spacing with grid dimensions was found and used for all of the nozzles for the particular scale. Table 3 provides the final dimensions and spacing chosen for the normal scale nozzles. The code was then extended to provide for the plume and co-flow regions. The source is provided in Appendix A.

Table 3: Normal scale interior grid dimensions

Dimension	
i_{max}	201
j_{max}	81
wall spacing	5.0 $(10)^{-6}$ mm
throat spacing	1.0 $(10)^{-5}$ mm

The code provided nozzle grids for the normal scale simulations. They were quickly generated by providing the code with the parameters of the half angle and exit angle for the conical and bell nozzles respectively. The different scales of the nozzles were created through a utility of Wind-US called GMAN. This utility could scale the lengths of the grid including the mesh in both x- and y-directions, maintaining the angles which define the overall shape of the nozzle.

A grid independence study was conducted through the use of the Wind-US capability of grid sequencing. Sequencing refers to the level of coarsening of the grid. The sequencing of the grid by 1 X 1 means every other grid point is removed

from the original grid. Sequencing by 2 X 2 means every other grid point is removed from the 1 X 1 grid. Fig. 6 shows the difference between the efficiencies achieved at each sequencing level throughout the normal scale, conical nozzle study. There is substantial difference between the two sequenced curves as the laminar boundary layer is poorly resolved at 2 X 2 sequencing level. The results of no sequencing still shows modest differences from the 1 X 1 sequencing. One linear derivitive extrapolation suggests the next sequence of grid refinement would lead to efficiencies differences less than 0.5% of the current results. So, best estimates of nozzle performance are $\sim$ 1.0% below the no sequencing curves. Another observation from Fig. 6 is that for these grid sizes, the optimum half angle with respect to efficiency does not change. It is assumed that further refinement of the grid would not alter from this finding.

Performing the Simulations

Once the grids were created, the running of the simulations could be handled by Wind-US and its utilities. Boundary conditions were set using the GMAN utility. All the inputs such as flow conditions and numerical schemes were provided through the use of a data file. A sample data file is provided in APPENDIX B. This data file would contain keywords recognized by the code. Better understanding of these keywords and their function can be found at Ref. 16. Local time-stepping was used for all the studies. After a converged solution was found, a global, time-accurate run of the normal scale conical nozzle was performed to check for unsteadiness in the thrust. The viscosity model was set using one of these keywords. The Reynolds number based on nozzle throat of 2380 for the original optimization study of Ref. 14 suggests the flow is safely laminar. The Reynold's number is defined by Equation 2.

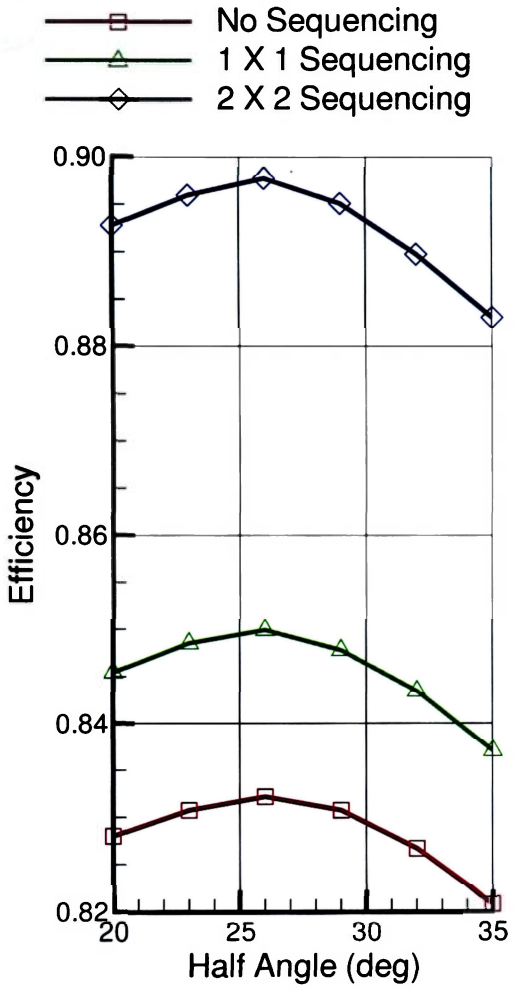

Figure 6: Sequencing plots for grid independence of conical nozzles

$$Re = \frac{\rho u D_H}{\mu} \tag{2}$$

Another important aspect of the data file is defining the freestream pressure representing the flow outside the nozzle. A perfect vacuum back pressure cannot be imposed in a continuum flow solution, so a finite back pressure is specified. Due to stability issues arising from high pressure differences (150 kPa to vacuum), the freestream pressure would be set at a less agressive value (1.0 psi), and the flowfield would be allowed to settle to nearly steady conditions. The freestream value would then be decreased on a re-start of the code, utilizing the data from the higher

freestream value. Due to numerical stability issues and desire to run a matrix of flow conditions, a relatively conservative choice of 0.01 psi (69 Pa) was chosen as the final freestream value for all the optimization study simulations.

Post-processing of the data was handled through another utility of Wind-US called CFPOST. This utility could provide value of a large number of variables through the flowfield. CFPOST also provided thrust values obtained from momentum and pressure values at the exit plane of the nozzle. Plot3D files were also provided for visual ispection of the flowfield through the use of Tecplot.

RESULTS

Experimental and Numerical Comparison

Because of the high Reynold's number mentioned before for this case, simulations using laminar viscosity and Menter's shear stress transport model were conducted. However the thrust and flow patterns are negligibly different. As expected. the boundary layer is quite small due to higher Reynold's numbers. At sea-level conditions the nozzle is highly overexpanded and this leads to the large dead flow region within the nozzle as seen in Fig. 7. The vacuum results (Fig. 8) show high expansion of the flow resulting in the expected high efficiency. The thrust efficiencies are listed in Table 4 along with the corresponding thrust stand results. The numerical thrusts and efficiencies are roughly 25% larger than the experimental values. Although various potential thrust losses have been considered experimentally, the source of the bulk of this discrepancy remains unclear and a topic of future investigation.

Table 4: Experimental and Numerical Nozzle Efficiency Comparison

Ambient Conditions	η : Test Stand (Exp)	η : Wind-US (Num)	Ratio (Exp/Num)
Sea Level	0.437	0.596	0.756
Vacuum	0.705	0.932	0.733

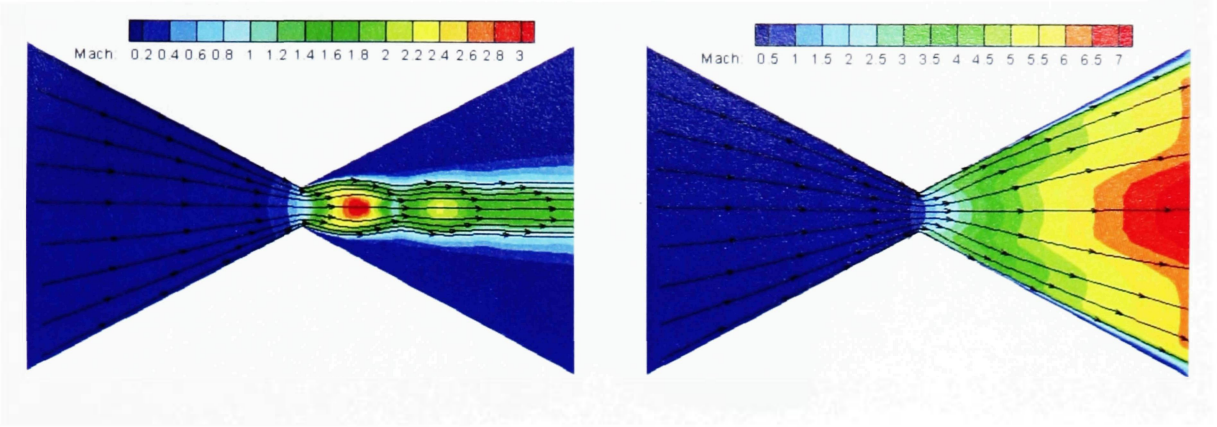

Figure 7: CFD result of experiment under sea level conditions

Figure 8: CFD result of experiment under vacuum conditions

Outflow Study

The resulting Mach contours for three different treatments of the outflow boundary are provided in Figs. 9 through 11, along with corresponding predicted thrust efficiency levels in Table 5. The efficiency is defined as the actual thrust divided by the ideal thrust,

$$\eta = F_{t,actual}/F_{t,ideal} \tag{3}$$

where the ideal thrust is based on assumption of 1-D, isentropic expansion to the nozzle exit for a fixed expansion ratio.

The flowfield result provided in Ref. 14 was first duplicated using a pure extrapolation everywhere at the outflow boundary. The recirculation shown in Fig. 9 is caused by a relatively high pressure ($\sim$ 0.18 psi) established in the large subsonic region near the nozzle exit. This high pressure causes the nozzle to behave as if overexpanded since ideally the nozzle could expand to a pressure of 0.007 psi. An impossible thrust value is obtained for the pure extrapolation case. However, it must be emphasized that while operating in a vacuum, this back pressure is not a realistic prediction of the boundary behavior.

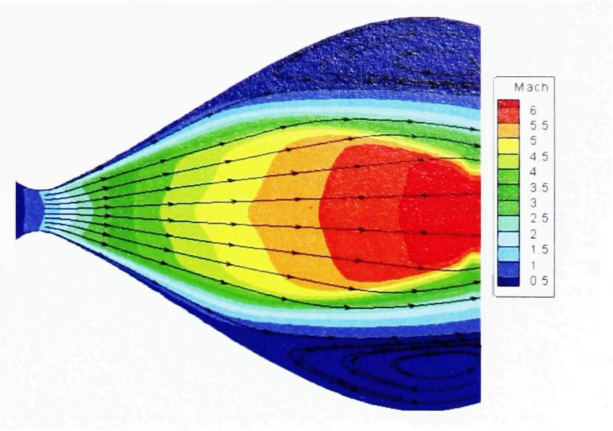

Figure 9: Initial study results using pure extrapolation

The next outflow boundary condition applied featured a mixture of extrapolation (where supersonic) and a prescribed back pressure (where subsonic). Fig. 10 illustrates the Mach contours for the mixed treatment including a back pressure of 0.01 psi. Although a converged result is obtained, unphysical behavior occurs where the flow switches from subsonic to supersonic flow. We found that this odd numerical behavior does not occur for conical nozzles of similar size under same flow conditions. It is not clear what conditions are necessary for this outflow treatment to fail in this manner. Regardless, the assumption of a constant pressure for the relatively large subsonic region at the nozzle exit is ambiguous at best. If a 0.20 psi back pressure is imposed, the resulting Mach contours (not shown) are very similar to those in Fig 9. Note that the thrust level is also greatly reduced compared to pure extrapolation case since the freestream pressure must be subtracted from the pressure term in the thrust calculation.

The final treatment sought to eliminate the nozzle outflow boundary. Two additional zones were implemented to resolve the nozzle plume (i.e., co-flow and downstream regions). Fig 11 illustrates the Mach contours for the vicinity of the nozzle for this 3-zone grid. The domain stretches 40 nozzle exit diameters downstream and 10 diameters radially outward. The Mach contours indicate that

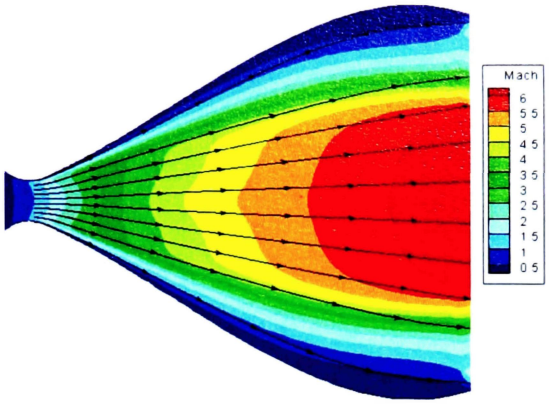

Figure 10: Initial study results using mixed extrapolation

the flow is under-expanded at the nozzle exit due to flow turning outward downstream of the nozzle trailing edge lip. The resulting thrust prediction in Table 5 differs from either of the previous two attempts, but compares much better with the case with imposed back pressure of 0.01 psi, as expected. This 3-zone approach is more computationally intensive due to need to resolve plume and low ambient pressure/density, but a sufficiently low freestream pressure can be imposed to ensure accurate thrust predictions and numerical stability. The Isp for the multi-zone case is 569 s.

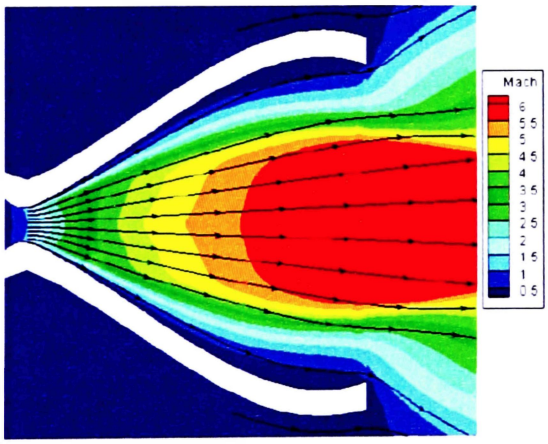

Figure 11: Initial study results using three zones

Table 5: Performance sensitivity to outflow settings

Outflow treatment	T_0 (K)	P_0 (MPa)	$\dot{m}$ (kg/s)	F_t (N)	η
Ideal	1500	0.150	$2.28\ (10)^{-5}$	0.145	1
Pure extrapolation	1500	0.150	$2.17\ (10)^{-5}$	0.152	> 1
Mixed extrapolation (69 Pa)	1500	0.150	$2.14\ (10)^{-5}$	0.117	0.807
Multi-zone (69 Pa)	1500	0.150	$2.15\ (10)^{-5}$	0.120	0.828

Conical Nozzle Study

The first optimization study from Ref. 14 involved the cone shaped nozzle. Fig. 13 shows how thrust efficiency (as defined earlier) varies with half angle and geometric scale. The original scale is the size indicated in Table 1. The thrust efficiency increases substantially with increases in scale. This is due to increases in Reynolds number and related reduction in influence of viscous effects (i.e., reduced boundary layer growth). Figures 14 17 provide Mach contours for these optimal half angles for their respective scales. They provide visual evidence of the effect scale has on boundary layer growth. Additionally, the time-accurate simulations of the normal scale revealed no variation in thrust due to momentum changes.

The optimal half angle of 26° for the original scale agrees with the findings in Ref. 14. The shows evidence of compatability between our study with the one performed by Shebalin and Tiwari. Fig. 13 also reveals the optimum performance occurs at conical half angles of about 38°, 29°, 26°, and 23° for the quarter, half, original, and double scales, respectively. Optimal conditions exist due to the minimization of the two most important losses for such a nozzle, divergence and boundary-layer effects. Divergence losses occur in a nozzle when the exhaust velocity has a non-axial component, which does not result in axial thrust development. For a conical nozzle where the flow must leave at an angle to the axial direction close to the nozzle walls, these losses are unavoidable. To reduce

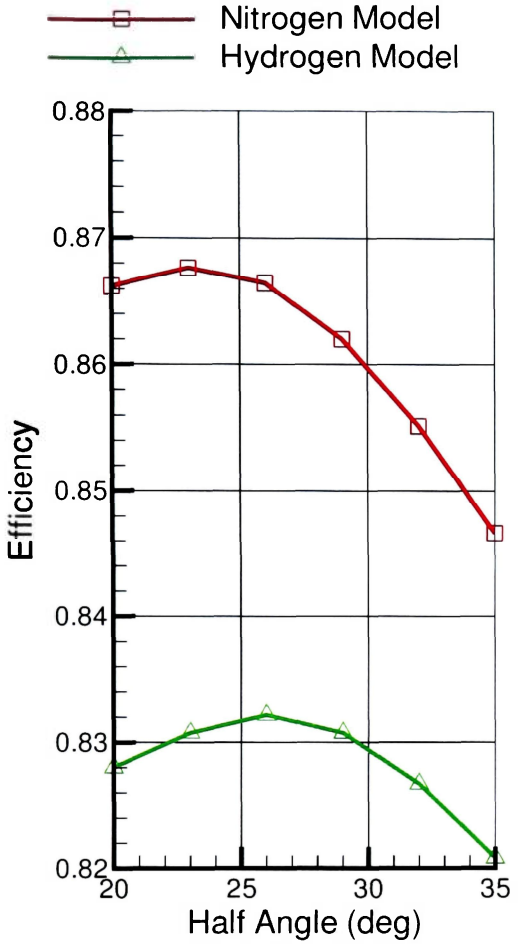

Figure 12: Efficiency versus half angle for conical nozzle with varying species

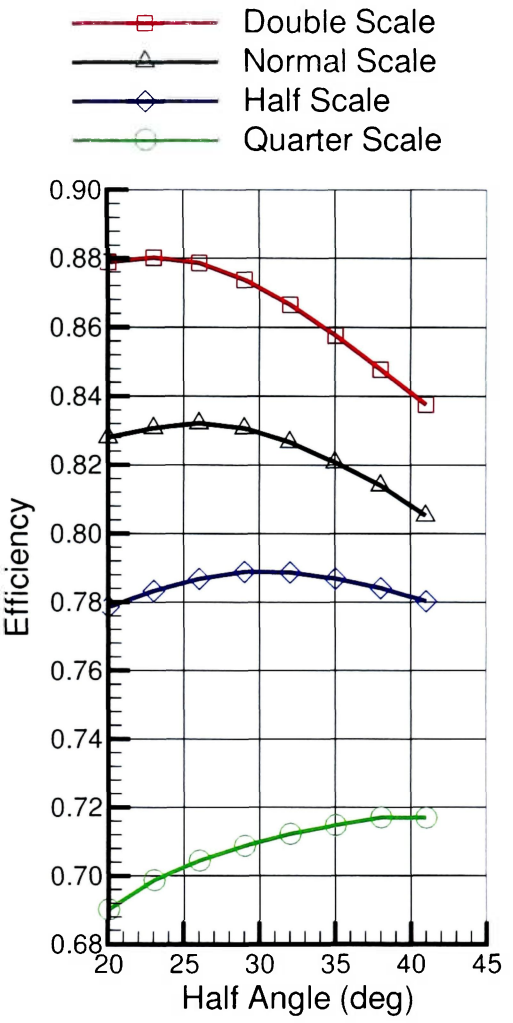

Figure 13: Efficiency versus half angle for conical nozzle and different scales

divergence losses, the cone angle is reduced, which results in a longer nozzle length to meet constant diameter restriction. However, the long nozzle increases the boundary layer and displacement thickness growth. The nozzle's effective expansion ratio is reduced as the boundary layer becomes larger, resulting in reduced thrust. Consequently, there is an optimal cone angle to minimize total thrust loss, balancing the divergence losses with the losses due to the boundary layer.

Fig. 12 illustrates the effect of chemical specie on the thrust efficiency. Replacing hydrogen with nitrogen for the same operating conditions results in approximately

doubling of Re* (i.e., by factor of 1.88) and a significant increase in efficiency of 3.5%. This increase can be compared to the 4.7% increase in efficiency for doubling Reynolds number via geometric scale.

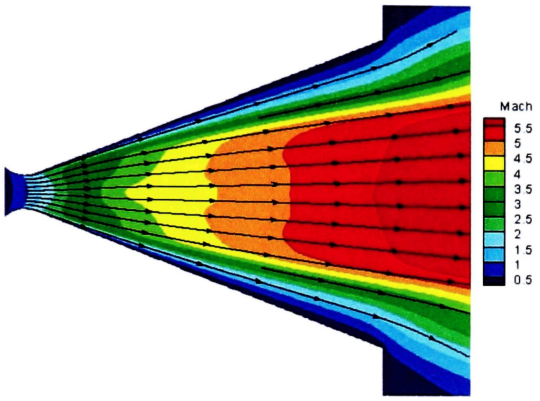

Figure 14: Double scale cone nozzle

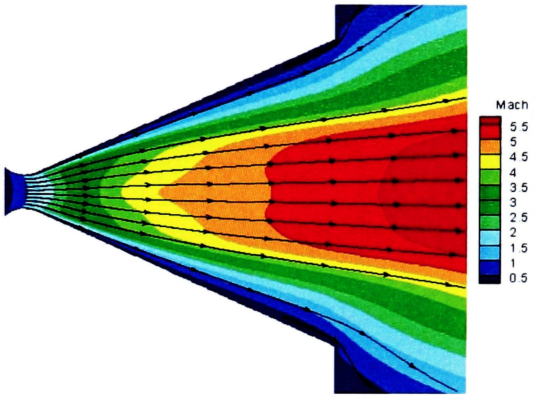

Figure 15: Normal scale cone nozzle

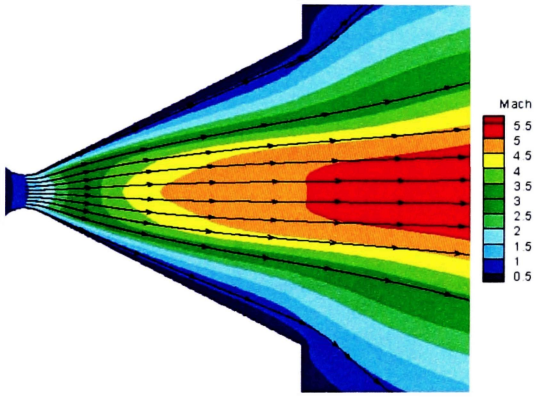

Figure 16: Half scale cone nozzle

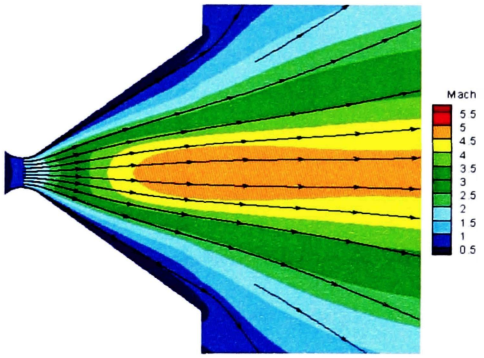

Figure 17: Quater scale cone nozzle

Bell Nozzle Study

Similar plots show the effect of shape, scale and propellent species effects the nozzle performance of bell nozzles. Fig. 19 shows how thrust efficiency varies with exit angle and geometric scale. The thrust efficiency increases substantially with

increases in scale due to increases in Reynolds number, and related reduction in influence of viscous effects (i.e., reduced boundary layer growth).

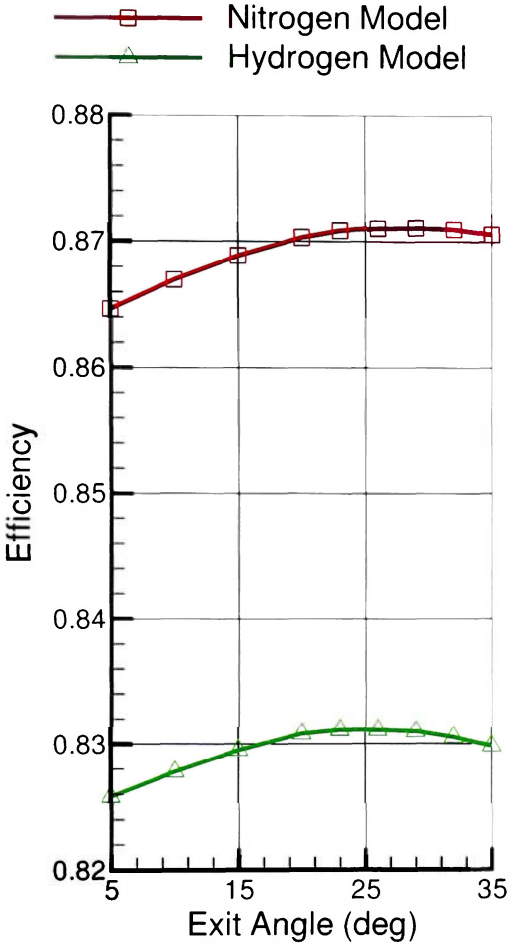

Figure 18: Efficiency versus exit angle for bell nozzle with varying species

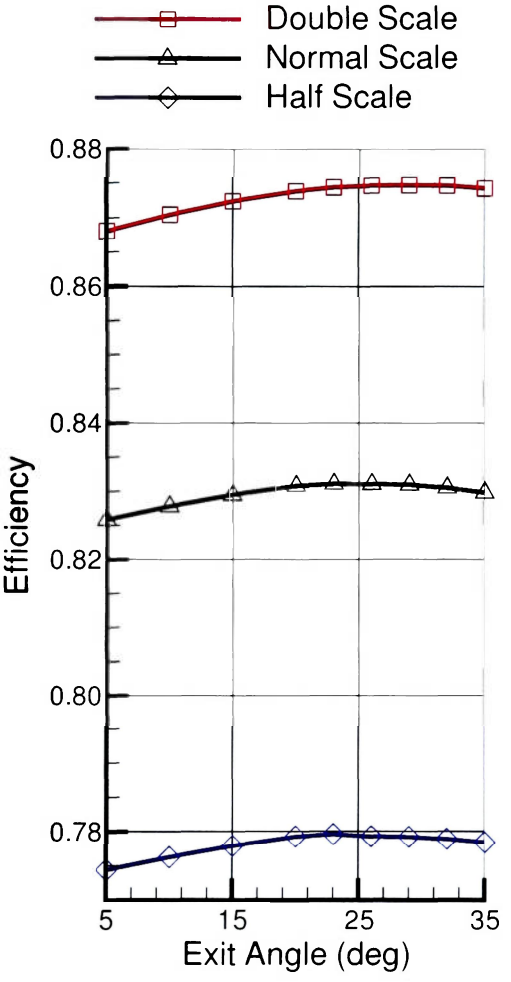

Figure 19: Efficiency versus exit angle for bell nozzle and different scales

Fig. 19 also shows that the optimum performance occurs near a nozzle exit angle of 26°, for the half, original, and double scales. The curves are nearly flat in the vicinity of each optimum, and within a few tenths of variation, the optimum angle is the same at the inflection angle of 26°. The reason is related to minimizing boundary layer growth. A curved bell nozzle adds arc length for a boundary layer to grow. A conical nozzle provides the shortest wall length and thus tends to minimize

boundary layer growth. So, it appears that the optimal bell nozzle for microthruster applications is very close to a conical nozzle, which would be beneficial to micronozzle builders due to the difficulties of machining complex contours in such small nozzles. Mach contours in Figures 20 - 22 show the effect of scale on boundary layer growth for bell nozzles of 0° exit angle, since the optimal bell nozzles would resemble the conical results.

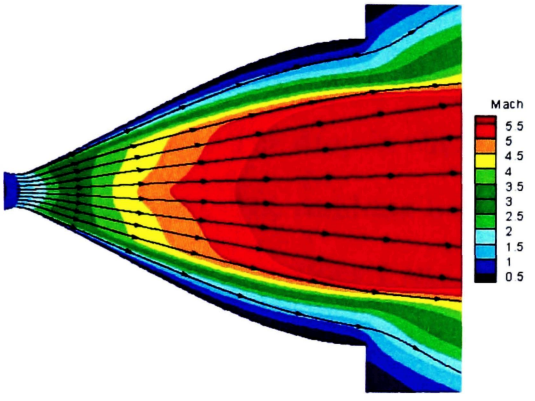

Figure 20: Double scale bell nozzle

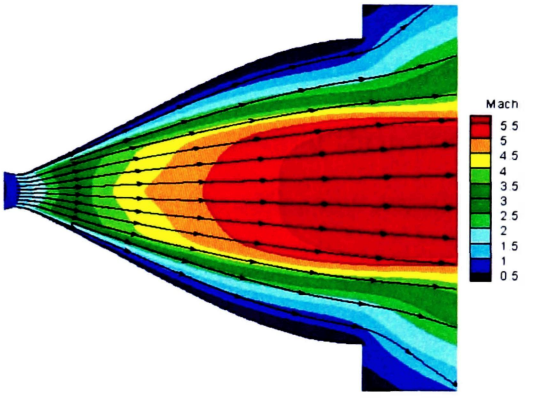

Figure 21: Normal scale bell nozzle

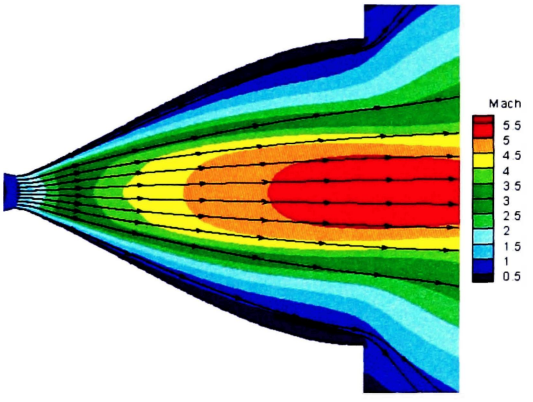

Figure 22: Half scale bell nozzle

Fig. 18 includes comparison of thrust predictions using either hydrogen or nitrogen single-specie gas propellants to provide additional sensitivity data versus Re^*. Replacing hydrogen with nitrogen for same operating conditions results in approximately doubling Re^* (i.e., factor of 1.88) and a significant increase in

efficiency of 4%. This increase can be compared to the 4.2% increase in efficiency for doubling Re~ via geometric scale.

Correlations

Correlations for the thrust efficiency versus Re* are developed based on the optimal hydrogen conical and bell nozzle results at each of the scales plus additional nitrogen normal scale result (i.e., based on 4-5 data points each). Fig. 23 illustrates how the efficiency drops with decreasing Re*. The curves for conical and bell nozzles are quite similar. The drop in efficiency represents a loss of potential thrust or loss of maximum Isp. The resulting best-fit power curve for thrust efficiency versus Re* is listed below in Equations 4 and 5 for the conical and bell nozzles repectively. Fig. 24 provides the related curve for the optimal conical half angle versus Re* defined by Equation 6. Although not developed based on 3-D MEMs-type linear nozzles, this correlation should apply to such nozzles using hydraulic diameter to calculate the throat Reynolds number. Rectangular nozzles are known to produce corner effects which would further reduce performance compared to axisymmetric nozzles, and so, this correlation would provide an upper bound on performance.

$$\eta = 0.400 Re^{*(0.093)} \tag{4}$$

$$\eta = 0.434 Re^{*(0.083)} \tag{5}$$

$$\theta = 170.6 Re^{*(-0.239)} \text{ degrees} \tag{6}$$

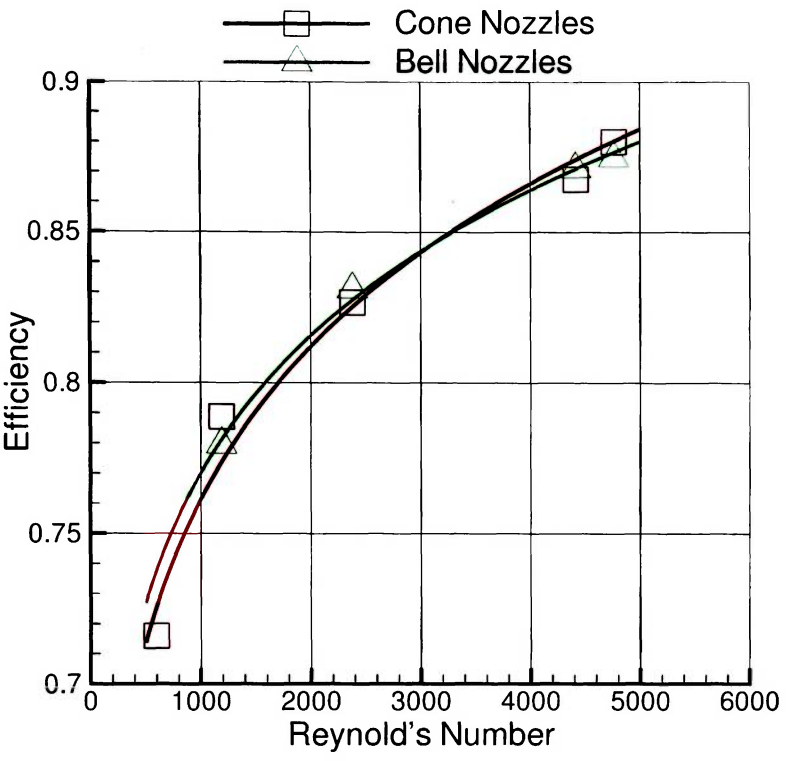

Figure 23: Optimal efficiency against Reynold's number

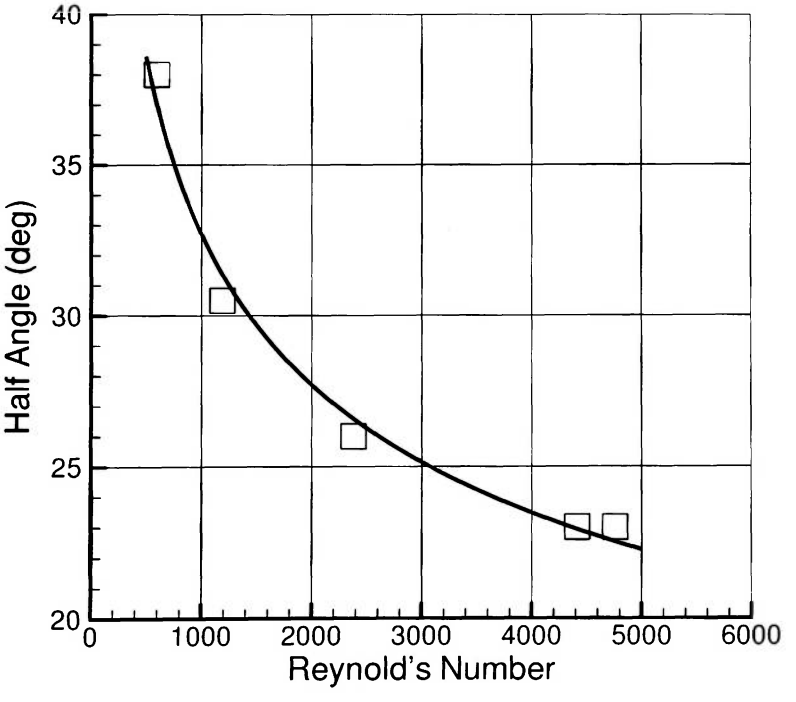

Figure 24: Optimal conical half angle against Reynold's number

CONCLUSIONS

The first section of the study focused on the simulation of micronozzles to be compared with experimental data. Unfortunately as seen in the experimental community at large, the obtaining of reliable results for comparison is difficult at best. There was an approximately 25% reduction in efficiency for the experimental results when compared to the numberical results. At this current time, there is no diffinitive explanation for this discrepency.

Analysis of the opitmal bell nozzle obtained by Shelbalin and Tiwari revealed a nessessity of simulating the plume region in addition to the interior nozzle flow to capture the expansion of the propellent. As such, a new optimization study was conducted using a grid containing a zone for the plume in place of a single zone interior flow grid.

When conducting the new optimization study, a trend appears regarding the efficiency of the micronozzle with regard to the Reynold's number. For the Reynold's number values in this study, decreasing the Reynold's number dramatically decreases the efficiency of the nozzle. This effect can be seen through the scaling of the micronozzles themselves and through the use of different monopropellent. In the case of the conical nozzles, Reynold's number also has an effect on the optimal half angle. The bell nozzle's shape is also influenced by the low Reynold's number values by ultimately reverting the contour shape into a conical one and thus reducing the viscous losses. Correlations relating the efficiency and

optimal nozzle shape as influenced by Reynold's number have been determined for nozzles with these specific design constraints.

As evident in current literature and this study, there are certainly more possibilities to consider in the design of micronozzles. For this optimization study, the nozzles were basically limited to nozzles with an expansion ratio of 82. A variable expansion ratio could be another parameter to consider. In such a study, the total length of the conical nozzles might be fixed to meet a certain design criteria. Changing the characteristics of the propellant species may be another valid expansion of this study including chemically reacting and thermally perfect flow. Reliable experimental analysis and results however would be the greatest enhancement to validating the findings of this study. Clearly several possibilities beyond this study still exist for investigation.

REFERENCES

1. Alexeenko, A. A., Gimelshein, S.F., Levin, D.A., Collins, R.J., "Numerical Modeling of Axisymmetric and Three-Dimensional Flows in MEMS nozzles." AIAA-2000-3668.

2. Bayt, R.L., "Analysis, Fabrication and Testing of a MEMS-based Micropropulsion System," MIT, Dissertation, June 1999.

3. Cubesat standard web page, Cal Poly, `http://cubesat.atl.calpoly.edu/pages/documents.php`. accessed May 24, 2007.

4. Engblom, W. A., O'Gara, M. R., et.al., "Investigation of Microthruster Nozzle Performance for Nanosatellite Applications," AIAA-2007-3985.

5. Hussaini, M. M., and Korte, J. J., "Investigation of Low-Reynolds-Number Rocket Nozzle Design Using PNS-Based Optimization Procedure," NASA TM-110295, 1996.

6. Jones, J. R., Mattick, A. T., "MEMS Micronozzle Flow Analysis of a High-Temperature Chemical Propulsion System," AIAA-2003-6270.

7. Ketsdever, Andrew D. "System Considerations and Design Options for Microspacecraft Propulsion Systems" *Micropropulsion for Small Spacecraft, AIAA Progress in Astronautics and Aeronautics*, Vol. 187, 2000, Chpt 4, pp. 139-163.

8. Louisos, W.F., Hitt, D.L., "Heat Transfer and Viscous Effects in 2D & 3D Supersonic Micro-Nozzle Flows," AIAA-2007-3987.

9. Louisos, W.F., Hitt, D.L., "Optimal Expansion Angle for Viscous Supersonic Flow in 2-D Micro-Nozzles," AIAA-2005-5032.

10. Mueller, Juergen. "Thruster Options for Microspacecraft: A Review and Evaluation of Existing Hardware and Emerging Technologies" *Micropropulsion for Small Spacecraft, AIAA Progress in Astronautics and Aeronautics*, Vol. 187, 2000, Chpt 3, pp. 45-137.

11. Nelson, C.C. and Power, G.D., "CHSSI Project CFD-7: The NPARC Alliance Flow Simulation System," 2001-0594, Jan. 2001.

12. Rao, G. V. R., "Exhaust Nozzle Contour for Optimum Thrust," Proceedings of the ARS Semi-Annual Meeting, San Francisco, CA, June 1957.

13. Rhee, M.S., C.M. Zakrzwski, and M.A. Thomas, "Highlights of Nanosatellite Propulsion Development Program at NASAGoddard Space Flight Center," 14th Annual AIAA/USU Conference on Small Satellites, 2000, SSC00-X-5.

14. Shebalin, J-P, and Tiwari, S. N., "NOZ-OP-2D: A CFD-based Optimization System for Axially Symmetric Rocket Nozzles," AIAA-2001-1062.

15. Storck, W., Billett, O., Cutler, J., Jambusaria, M., Sadhwani, A., and Jammes, P., "A Survey of Micropropulsion for Small Satellites," 20th Annual AIAA/USU Conference on Small Satellites, 2006, SSC06-VIII-3.

16. Wind-US User's Guide, Glenn Research Center, `http://www.grc.nasa.gov/WWW/winddocs/user/index.html`, accessed October 1, 2007

APPENDIX A

GRID GENERATION CODE

```
! Program to calculate the contour of a 'optimized' micronozzle
! based for a contoured micronozzle

! Michael O'Gara
! Source: Shebalin and Tiwari, Old Dominion University, 2001

! Optimized Nozzle Geometry Info
! Values are in meters until conversion at the end

PROGRAM nozzle
IMPLICIT none

! Parameters and measurements from Shebalin and Tiwari
REAL*8, PARAMETER :: pi = 3.14159
REAL*8, PARAMETER :: r_star = 0.00042
REAL*8, PARAMETER :: A_by_A_star = 82.0
REAL*8, PARAMETER :: R_curve = 1.5*r_star ! throat curvatue
REAL*8, PARAMETER :: theta_infl = 26.0/180.0*pi ! for contoured nozzles

! User Defined Values
INTEGER :: contour ! 2 = conical nozzle 1 = bell nozzle

REAL*8, PARAMETER :: throat_cell = 1.0E-5 ! dimension of first cell off of
REAL*8, PARAMETER :: wall_cell = 5.0E-6 ! throat and wall location (meter)
REAL*8 :: theta_exit !----------to be defined interactively
INTEGER, PARAMETER :: x_dim = 201
INTEGER, PARAMETER :: y_dim = 81
INTEGER :: throat_dim = x_dim/5 ! this seemed to work well
CHARACTER(LEN=20) :: output_file

! zone 2 and 3 options
INTEGER :: x_dim2 = 121
INTEGER :: y_dim2 = 161
INTEGER :: x_dim3 = 30
INTEGER :: y_dim3 = 10

REAL*8 :: A, B, C, D
REAL*8 :: x_exit, y_exit
REAL*8 :: x_circle, y_circle
REAL*8 :: x1, y1, A1, A2, A3, H, zone2x, zone2y
INTEGER :: i, j, n, m, i_curve
REAL*8 :: realnum, s, s1, s2, s3, sum, Ax, Ay
REAL*8 :: exit_space, top_y, far_x, real_y
REAL*8, ALLOCATABLE, DIMENSION(:) :: X, X2, Y3, Y2, Y4, Y5, X3
REAL*8, ALLOCATABLE, DIMENSION(:,:) :: Y
```

```
ALLOCATE(X(x_dim), Y(x_dim,y_dim), X2(x_dim2), X3(x_dim3))

PRINT *, "WHAT SHAPE SHOULD THE NOZZLE BE?"
PRINT *, ""
PRINT *, " 1 = BELL , 2 = CONE"
READ *,contour

IF (contour /= 1) THEN
IF (contour /= 2) THEN
PRINT *, "THAT IS NOT A VALID INPUT"
STOP
END IF
END IF

PRINT *, "NAME THE OUTPUT FILE WITH .x EXTENSION ATTACHED"
READ '(A)',output_file

IF (contour == 1) THEN
PRINT *,"What exit angle is desired (degrees)?"
ELSE
PRINT *,"What half angle is desired (degrees)?"
END IF

READ *,theta_exit
theta_exit = theta_exit/180.0*pi

! Calculation of the starting point for the nozzle

x1 = -R_curve*sin(theta_infl)
y1 = (R_curve+r_star)   R_curve*cos(theta_infl)

! Calculation for end of throat curvature

x_circle = R_curve*sin(theta_infl)
y_circle = (R_curve+r_star)   R_curve*cos(theta_infl)

! Calculation for end of nozzle

y_exit = r_star*sqrt(A_by_A_star)
IF (contour == 1) THEN
x_exit = 0.007899 ! set by Shebalin and Tiwari
ELSE
x_exit = x_circle + (y_exit-y_circle)/tan(theta_exit)
END IF
```

```
top_y = y_exit*10.0
far_x = y_exit*30.0

! Make throat dimensions divisible by 2
realnum = throat_dim
IF (realnum/2.0 /= throat_dim/2) throat_dim = throat_dim + 1

! Solve for Coefficients of Bell Nozzle Contour

IF (contour == 1) THEN
A = y_circle
B = tan(theta_infl)

C = 3.0*(y_exit-y_circle-(x_exit-x_circle)*B)/(x_exit-x_circle)**2.0
C = C - (tan(theta_exit) - B)/(x_exit-x_circle)

D = (tan(theta_exit) - B)/(x_exit-x_circle)**2.0
D = D + 2.0*(y_circle-y_exit+(x_exit-x_circle)*B)/(x_exit-x_circle)**3.0
END IF

sum = 0
s = 1

DO
sum = sum + (1.2**s)*wall_cell
IF (sum >= top_y) THEN
top_y = sum
EXIT
END IF
s = s+1
END DO

y_dim2 = s + y_dim
y_dim3 = ((y_dim2-y_dim)/3) ! pretty much sets lip thickness

ALLOCATE(Y2(y_dim2), Y3(y_dim2), Y4(y_dim3), Y5(y_dim3))

real_y = y_dim2-1
exit_space = top_y/real_y

! Defining centerline x values
sum = 0

DO i = 1,throat_dim/2   2
```

```
sum = sum+i
END DO

A1 = (-x1   (throat_dim/2   1)*throat_cell)/sum

X(throat_dim/2) = 0 ! set throat center to x = 0
X(1) = x1
X3(1) = x1
X3(x_dim3) = x_exit
X(throat_dim/2+1) = throat_cell
X(x_dim) = x_exit

DO i = 1, throat_dim/2   2
n = throat_dim/2   i
s1 = throat_cell + A1*(i-1)
X(n) = X(n+1)   s1
END DO

sum = 0

DO i = 1,x_dim-throat_dim/2-1
sum = sum+i
END DO

A2 = ((x_exit   throat_cell)   (x_dim-throat_dim/2-1)*throat_cell)/sum

DO i = 1.x_dim-throat_dim/2-2
m = throat_dim/2 + 1 + i
s2 = throat_cell + A2*i
X(m) = X(m-1) + s2
END DO

sum = 0

DO i = 1,x_dim3-1
sum = sum+i
END DO

A2 = ((x_exit   x1) - (x_dim3-1)*s2)/sum

DO i = 1,x_dim3-2
m = x_dim3 - i
s3 = s2 + A2*i
X3(m) = X3(m+1)   s3
END DO
```

```
DO i = 1.x_dim
IF (X(i) > x_circle) THEN
i_curve = i
EXIT
END IF
END DO

! Defining nozzle wall contour

! Throat Curvature
DO i = 1,i_curve-1
Y(i,y_dim) = R_curve + r_star   sqrt(R_curve*R_curve-X(i)*X(i))
END DO

IF (contour == 1) THEN
! Third Order Wall curve
DO i = i_curve,x_dim-1
Y(i,y_dim) = A + B*(X(i)-x_circle) + C*((X(i)-x_circle)**2) + D*((X(i)-x_circle)**3)
END DO
ELSE
! Linear Conical Nozzle
DO i = i_curve,x_dim-1
Y(i,y_dim) = y_circle + (X(i)-x_circle)*tan(theta_exit)
END DO
END IF

Y(x_dim,y_dim) = y_exit

! Outer zone(s) defining

Y3(y_dim) = y_exit
Y3(y_dim2) = top_y
X2(1) = x_exit
X2(x_dim2) = far_x
Y(:,1) = 0
Y3(1) = 0
Y2(1) = 0
Y2(y_dim2) = top_y

DO i = 2, y_dim2-1
Y2(i) = (exit_space)*(i-1)
END DO

sum = 0
```

```
DO i = 1,y_dim-2
sum = sum+i
END DO

DO i = 1,x_dim
Ay = ((Y(i,y_dim)-wall_cell)    (y_dim-2)*wall_cell)/sum
DO j = 1,y_dim-2
m = y_dim-j
s = wall_cell + Ay*(j-1)
Y(i,m) = Y(i,m+1)    s
END DO
END DO

DO i = 2,y_dim-1
Y3(i) = Y(x_dim,i)
END DO

sum = 0

DO i = 1,x_dim2-1
sum = sum+i
END DO

Ax = ((far_x - x_exit) - (x_dim2-1)*s2)/sum
DO j = 1,x_dim2-1
s = s2 + Ax*(j)
X2(j+1) = X2(j) + s
END DO

sum = 0

DO i = 1,y_dim2    y_dim    1
sum = sum+i
END DO

DO j = y_dim+1,y_dim2-1
s = wall_cell*(1.2)**(j-y_dim)
Y3(j) = Y3(j-1) + s
END DO

DO i = 1,y_dim3
Y4(i) = Y3(i + y_dim2 - y_dim3)
END DO
```

```
DO i = 1, y_dim3
Y5(i) = Y4(i)
END DO

OPEN (UNIT=8,FILE=output_file,STATUS="NEW")
WRITE (UNIT=8,FMT=*) 3
WRITE (UNIT=8,FMT=*) x_dim,y_dim,1
WRITE (UNIT=8,FMT=*) x_dim2,y_dim2,1
WRITE (UNIT=8,FMT=*) x_dim3,y_dim3,1

DO n = 1,y_dim
DO i = 1,x_dim
WRITE (UNIT=8,FMT=*) X(i)*39.37 ! meter to inch conversion
END DO
END DO

DO n = 1,y_dim
DO i = 1,x_dim
WRITE (UNIT=8,FMT=*) Y(i,n)*39.37 ! meter to inch conversion
END DO
END DO

DO n = 1,y_dim
DO i = 1,x_dim
WRITE (UNIT=8,FMT=*) 1.0 ! WIND axisymetric requirement
END DO
END DO

DO n = 1,y_dim2
DO i = 1,x_dim2
WRITE (UNIT=8,FMT=*) X2(i)*39.37 ! meter to inch conversion
END DO
END DO

zone2x = far_x   x_exit
DO n = 1,y_dim2
zone2y = Y3(n)-Y2(n)
WRITE (UNIT=8,FMT=*) Y3(n)*39.37 ! meter to inch conversion
DO i = 2,x_dim2-1
H = Y3(n) + (x_exit-X2(i))*zone2y/zone2x
WRITE (UNIT=8,FMT=*) H*39.37 ! meter to inch conversion
END DO
WRITE (UNIT=8,FMT=*) Y2(n)*39.37 ! meter to inch conversion
END DO
```

```
DO n = 1,y_dim2
DO i = 1,x_dim2
WRITE (UNIT=8,FMT=*) 1.0 ! WIND axisymetric requirement
END DO
END DO

DO n = 1,y_dim3
DO i = 1,x_dim3
WRITE (UNIT=8,FMT=*) X3(i)*39.37 ! meter to inch conversion
END DO
END DO

zone2x = x_exit - x1

DO n = 1,y_dim3
zone2y = Y4(n)-Y5(n)
WRITE (UNIT=8,FMT=*) Y5(n)*39.37 ! meter to inch conversion
DO i = 2,x_dim3-1
H = Y5(n) + (X3(i)-x1)*zone2y/zone2x
WRITE (UNIT=8,FMT=*) H*39.37 ! meter to inch conversion
END DO
WRITE (UNIT=8,FMT=*) Y4(n)*39.37 ! meter to inch conversion
END DO

DO n = 1,y_dim3
DO i = 1,x_dim3
WRITE (UNIT=8,FMT=*) 1.0 ! WIND axisymetric requirement
END DO
END DO

ENDFILE 8

END PROGRAM nozzle
```

APPENDIX B

SAMPLE WIND-US INPUT FILE

```
WIND micro-nozzle, axisymmetric, 2 zones
Supersonic internal flow w/ plume
Run 1

/ Inlet conditions
FREESTREAM total 0.1 0.010 540. 0. 0.
hold characteristics zone 1:2

/ Specified Gas Parameters
GAS 1.4 0.678 0.92 24662.

SEQUENCE 0 0 0 ZONE 1:2

ARBITRARY INFLOW
TOTAL
HOLD_TOTALS
DIRECTION along
ZONE 1
UNIFORM 0.10 21.756 2700. 0. 0.
DIRECTION normal
ENDINFLOW

/ Boundary conditions
DOWNSTREAM PRESSURE freestream extrapolate supersonic zone 2

AXISYMMETRIC 0.0 5.0

/ Numerics
Cycles 2000
Iterations per cycle 5 Print frequency 5
/cfl# cfl 0.5
cfl# mode 2 cfl increment 0.1 0.5 1.1 1 1 zone 1:3

CONVERGE ORDER 10

/ Viscous terms
TURBULENCE LAMINAR

VISCOSITY custom 1.07361E-08 174.6

/ Explicit Order Operator
RHS roe second physical
/RHS roe first upwind
```

```
/ Specified Loads
LOADS
pressure offset 0
print planes frequency 50
reference area 1
reference length 1
ZONE 1
surface I last mass force momentum
ENDLOADS
```